Structural Basis and Binding Properties of the Second Bromodomain of Brd4 with Acetylated Histone Tails[†,‡]

Ying Liu, Xiqing Wang, Jiahai Zhang, Hongda Huang, Bo Ding, Jihui Wu,* and Yunyu Shi*

Hefei National Laboratory for Physical Sciences at Microscale and School of Life Science, University of Science and Technology of China, Hefei, Anhui, 230026, People's Republic of China

Received January 29, 2008; Revised Manuscript Received April 18, 2008

ABSTRACT: Brd4 belongs to the BET family. It is a multifunctional protein involved in transcription, replication, the signal transduction pathway, and cell cycle progression. All of these functions are linked to its association with acetylated chromatin. With its tandem bromodomains, Brd4 avidly binds to diacetylated H4-AcK5/K12 and H3-AcK9/K14 peptides. Solution structure of the second bromodomain (BD) is reported in this research. In addition to the πD-helix, which is special for BET members, an incompact $\alpha Z'$ distinct from Brd2 BD2 is found, although they have identical sequences in this region. Both BD1 and BD2 bind to monoacetylated H4-AcK5 and H4-AcK12 peptides, but with subtle differences. An NMR perturbation study and mutational analysis identified the binding interface and revealed several residues important for binding specificity. By molecular dynamics simulations, a complex model composed of H4-AcK5/K12 and two molecules of BD2 is presented. Relaxation data and internal motions of BD2 are also discussed. Unlike Brd2 BD1, the two bromodomains of Brd4 are mainly monomeric in solution. They do not form heterodimers like TAFII250. It suggests that Brd4 should have its own mechanism to reinforce its chromatin association both in mitotic retention and related cellular regulation.

Bromodomain containing protein 4 (Brd4[1]) is a multifunctional protein and plays distinct roles through the interactions with different binding proteins. It regulates the activation of the transcription elongation process through interaction with core P-TEFb (*1–3*). It participates in the repression of replication and S phase entry through interaction with RFC (replication factor C) (*4*). Brd4 is also involved in the signal transduction pathway and G2 to M phase transition through interaction with SPA1 (*5*). Brd4 seems to associate with some forms of mediator complexes (*1, 6–9*). It also participates in the life cycle of some viruses, such as HIV (*1, 3*), KSHV (*10, 11*), HPV (*12–15*), and HTLV-1 (*16*). Significantly, all of these functions are linked to its association with acetylated chromatin through its two bromodomains.

Bromodomain (BD), an evolutionarily conserved protein module, has been identified to function as an acetyl-lysine (AcK) binding domain. Brd4 belongs to the BET (BD and extra C-terminal domain) family, a novel class of BD-containing proteins. The BET family includes mammalian Brd2, Brd3, Brd4, Brdt, *Drosophila* Fsh, yeast Bdf1, Bdf2, and corresponding homologues in other species (*9*). All of these proteins carry two tandem BDs, an ET (extra C-terminal) domain, motif A, B, and SEED (*9, 17*) (Figure 1). They not only have conserved domain organization but also share great sequence similarity within each domain. Brd4, Brdt, and Fsh also contain a CTD (C-terminal domain) important for functional protein targeting (*3, 9, 18*). Several putative PEST sequences may convey proteolytic signals and make Brd4 short-lived (*19, 20*).

Modifications on histone tails were hypothesized to form distinct histone codes. They provide different protein binding sites to direct molecular processes. Brd4 deciphers a specific histone code and then translates it into its own regulatory pathway. It was shown that Brd4 interacts with diacetylated histone H3 and/or H4 tails dynamically through its two BDs. This interaction associates Brd4 with chromatin in a rapid on and off mode throughout cell cycle progression (*21*). Brd4 persists on condensed chromosomes even in mitotic cells, whereas most of the chromatin binding proteins are dispersed into cytoplasm. It was proposed to mark the actively transcribed regions of the genome and transmit this reprogramming memory from one generation to the next (*21, 22*).

BDs of Brd4 have the highest sequence similarity with those of Brd2. Full length Brd2 was identified to form a homodimer through its BD1 in vitro and in vivo. The secondary pocket formed by dimerization significantly improves the binding affinity of Brd2 BD1 to H4-AcK12 (*23*). On the basis of the structure of Brd2 BD1, it was proposed that the two BDs of Brd4 also form heterodimers. Several amino acids in Brd4 are predicted to be involved in the homodimeric interface (*9*).

[†] This work was supported by the Chinese National Fundamental Research Project (Grant 2002CB713806, 2006CB806507 and 2006CB910201), the Chinese National Natural Science Foundation (Grant 30570361 and 30670426), and the National High-Tech R&D program (Grant 2006AA02A315).

[‡] The atomic coordinates have been deposited in the RCSB Protein Data Bank with accession code 2I8N. The NMR assignments have been deposited in the BioMagResBank with accession numbers 15057.

* To whom correspondence should be addressed. Tel: 86-551-3607464. Fax: 86-551-3601443. E-mail: yyshi@ustc.edu.cn (Y.S.); wujihui@ustc.edu.cn (J.W.).

[1] Abbreviations: BET, bromodomain and extra-terminal domain; Brd4, bromodomain containing protein 4; BD, bromodomain; PEST, proline (P), glutamic acid (E), serine (S), and threonine (T) rich sequence.

10.1021/bi8001659 CCC: $40.75
Published on Web 05/24/2008

FIGURE 1: Domain organization of human Brd4. Boundaries of the BD1, BD2, and ET domains are indicated by the numbers underneath.

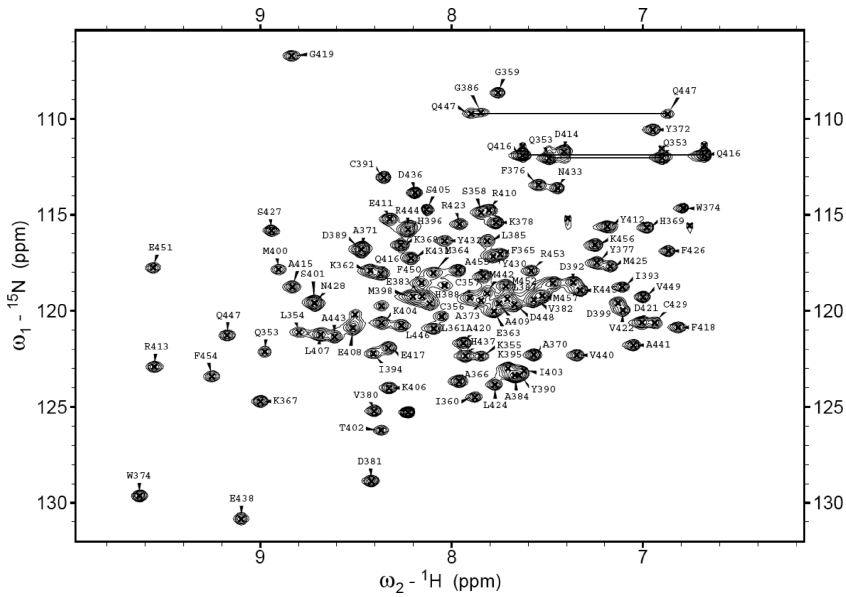

FIGURE 2: Two-dimensional ^{1}H-^{15}N HSQC spectrum of the wild-type Brd4 BD2. Assignments are indicated for the backbone NH pairs. Discernable peaks denoting amino groups from side chains of Q353, Q416, and Q447 were also labeled with a straight line between corresponding peak pairs.

Although significant progress has been made, the structural basis for the recognition of Brd4 and the specific histone code is still unknown. In this study, we determined the solution structure of Brd4 BD2 by NMR and investigated the binding characteristics of the two BDs for acetylated histone H3 and H4 peptides. An NMR perturbation study demonstrated that both BD1 and BD2 bound to peptides H4-AcK5 and H4-AcK12. No comparable perturbations were observed for unacetylated peptide controls. The dissociation constants (K_D) of BD1 and BD2 for H4-AcK5 and H4-AcK12, respectively, were measured. Mutational analysis revealed several residues important for binding specificity. A ternary complex model composed of H4-AcK5/K12 and two molecules of BD2 was proposed by molecular dynamics simulations. Dynamic properties of apo and ligand-bound BD2 are also discussed. Unlike Brd2 BD1, the two BDs of Brd4 are mainly monomeric in solution. They do not form heterodimers like TAFII250. It suggests that Brd4 should have its own mechanism to reinforce its chromatin association both in mitotic retention and related cellular regulation. The study provides meaningful insight into how Brd4 and other BET members recognize specific acetylated histone codes and thus impact related cellular processes.

MATERIALS AND METHODS

Expression, Purification, and Isotope Labeling of Brd4 Bromodomain. The DNA fragments, encoding Brd4 BD1 (49−166) and BD2 (352−457) of human Brd4 (NP_490597.1) were amplified by PCR from the human brain cDNA library (Clontech). The primers used are listed in Table SI-1. The amplified DNA fragments were subcloned into pET22b (+) (Novagen) and verified by sequencing the plasmids. Then the constructs were transformed into *E.coli* BL21 (DE3) Gold (Stratagene). Target protein expressions were induced at 289 K (BD1) for 24 h and 310 K (BD2) for 5 h. Uniformly ^{15}N

Table 1: Structural Statistics for the Family of 20 Lowest Energy Structures[a]

distance restraints	
intramolecular	1490
intraresidue ($i - j = 0$)	467
sequential ($\|i - j\| = 1$)	442
medium range ($2 \leq \|i - j\| \leq 4$)	411
long range ($\|i - j\| \geq 5$)	170
hydrogen bonds	54
total	1544
dihedral angle restraints	
φ	72
ψ	72
total	144
mean rms deviations from the experimental restraints	
distance (Å)	0.0042 ± 0.0004
dihedral (deg)	0.1652 ± 0.0137
mean rms deviations from idealized covalent geometry	
bond (Å)	0.0027 ± 0.00018
angle (deg)	0.3294 ± 0.0061
improper (deg)	0.1679 ± 0.0067
mean energies (kcal mol^{-1})	
Enoe	2.05 ± 0.41
Ecdih	0.24 ± 0.04
$E_{L\text{-}J}$	−406.09 +/− 11.00
Ramachandran plot[b]	
residues 1−106	
% residues in the most favorable regions	88.5
additional allowed regions	11.5
atomic rms differences (Å)[c]	
residues 1−106	
backbone heavy atom (N, C$^\alpha$, and C′)	0.704
heavy atoms	1.398

[a] None of the structures exhibits distance violations greater than 0.5Å or dihedral angle violations greater than 5°. [b] The program Procheck was used to assess the overall quality of the structures. [c] The precision of the atomic coordinates is defined as the average rms difference between the 20 final structures and the mean coordinates of the protein.

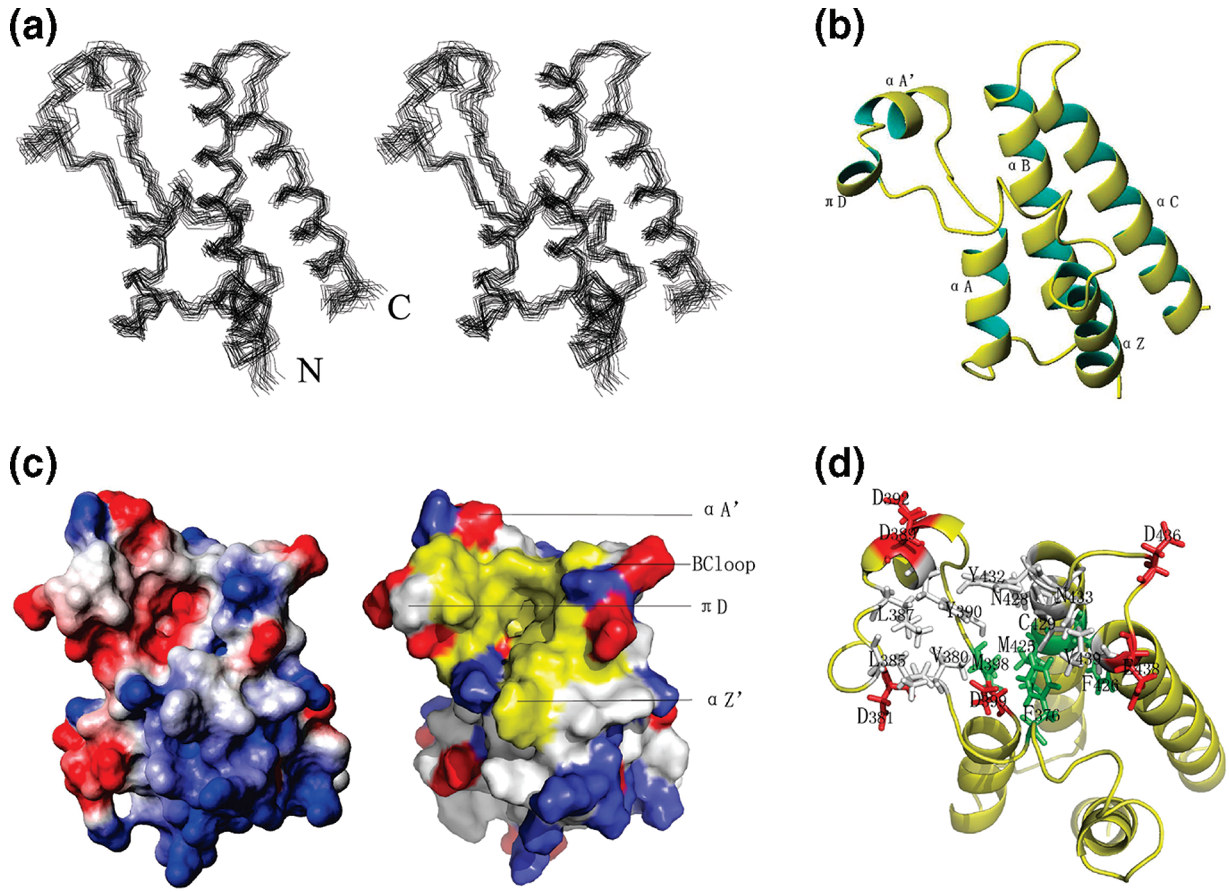

FIGURE 3: Three-dimensional solution structure and functional surface of Brd4 BD2. (a) Stereoview of the 20 representative conformers. (b) Ribbon representation of the energy-minimized structure with secondary structure elements highlighted. (c) Potential surface (left) and emphasized hydrophobic potential surface (right) of B at the acetyl-lysine binding site. Red denotes negative potential, blue positive potential, white hydrophobic potential, and yellow emphasized hydrophobic potential at the acetylated histone−peptide binding surface. (d) Side chain conformation of the residues surrounding the hydrophobic pocket.

and ^{13}C-labeled recombinant BDs were produced by growing the bacteria in SV40 medium using $^{15}NH_4Cl$ (0.5 g/L) and $^{13}C_6$-glucose (2.5 g/L) as the sole nitrogen and carbon source. The BDs were purified by Hitrapchelating column (Pharmacia) chromatography and FPLC size-exclusion column chromatography (HiLoad 16/60 Superdex 75 pg). The purity of the proteins was confirmed by SDS−PAGE, and the concentrations were measured with BCA reagent (Pierce).

Peptide Synthesis. Peptides used in the experiments were chemically synthesized using a standard Fmoc (*N*-9-fluorenyl methoxycarbonyl) method at Shanghai Sangon Biological Engineering & Technology and Service Co. Ltd.

FPLC Size-Exclusion Chromatography. Molecular weights of BDs (0.5 mM) were estimated in PBS solution (pH7.4) by a Superdex 75 10/300 GL column (Amersham Bioscience). The column was calibrated using proteins of known molecular weight: albumin (67 kDa), ovalbumin (43 kDa), chymotrypsinogen (25 kDa), and ribonuclease (13.7 kDa).

Analytical Ultracentrifugation (AUC). Sedimentation velocity studies were performed on a Beckman Optima XL-A analytical ultracentrifuge with an An60Ti rotor. Protein samples were buffered in PBS solution (pH7.4) and centrifuged at 56,000 rpm for 8 h. Absorbance scans were collected at a time interval of 3 min. Sedimentation profiles were analyzed with the software SEDFIT (version 8.9) using the continuous distribution c(s) Lamm equation model (*24, 25*).

NMR Experiments. NMR samples of Brd4 BD2 (1 mM) were buffered in 20 mM sodium phosphate, 50 mM NaCl, 5 mM EDTA, and 10 mM DTT in 90% H_2O and 10% D_2O (pH 6.0). NMR spectra were acquired at 293 K, on a Bruker DMX600 spectrometer with self-shielded *z*-axis gradients. The following spectra were recorded: 2D ^{1}H-^{15}N HSQC, ^{1}H NOESY, and ^{1}H TOCSY; 3D HNCO, HN(CA)CO, CBCA(CO)NH, CBCANH, C(CO)NH-TOCSY, H(CCO)NH-TOCSY, HCCH-TOCSY, HCCH-COSY, HBHA(CBCACO)NH, and ^{15}N- and ^{13}C- separated NOESY. To identify the slowly exchanging amides, the ^{15}N-labeled sample was lyophilized and dissolved in 99.96% D_2O, followed immediately by HSQC experiments to record the disappearance of NH signals. NMR data were processed by NMRPipe and NMRDraw software (*26*), and assigned with Sparky 3 (*27*).

Experimental Restraints and NMR Structure Calculation. NOE distance restraints were obtained from 3D ^{15}N-saperated NOESY and 3D ^{13}C-saparated NOESY spectra. Backbone dihedral angles (φ and ψ) in secondary structures were derived from analysis of $^{13}C\alpha$, $^{13}C\beta$, ^{13}CO, $^1H\alpha$, and ^{15}N chemical shifts by TALOS (*28*). Only TALOS good predictions, with 5 or 6 matches in agreement, were used. Hydrogen bond restraints were defined from the slow exchange amide protons mainly in the regular secondary structures. At a later stage of structure calculation, only hydrogen bonds whose donors could be identified unambiguously were added. The structures were calculated with a simulated annealing protocol using the CNS v1.1 program (*29*). In the final calculations, 200 structures were generated, from which 20 models with lowest energies were selected to form the

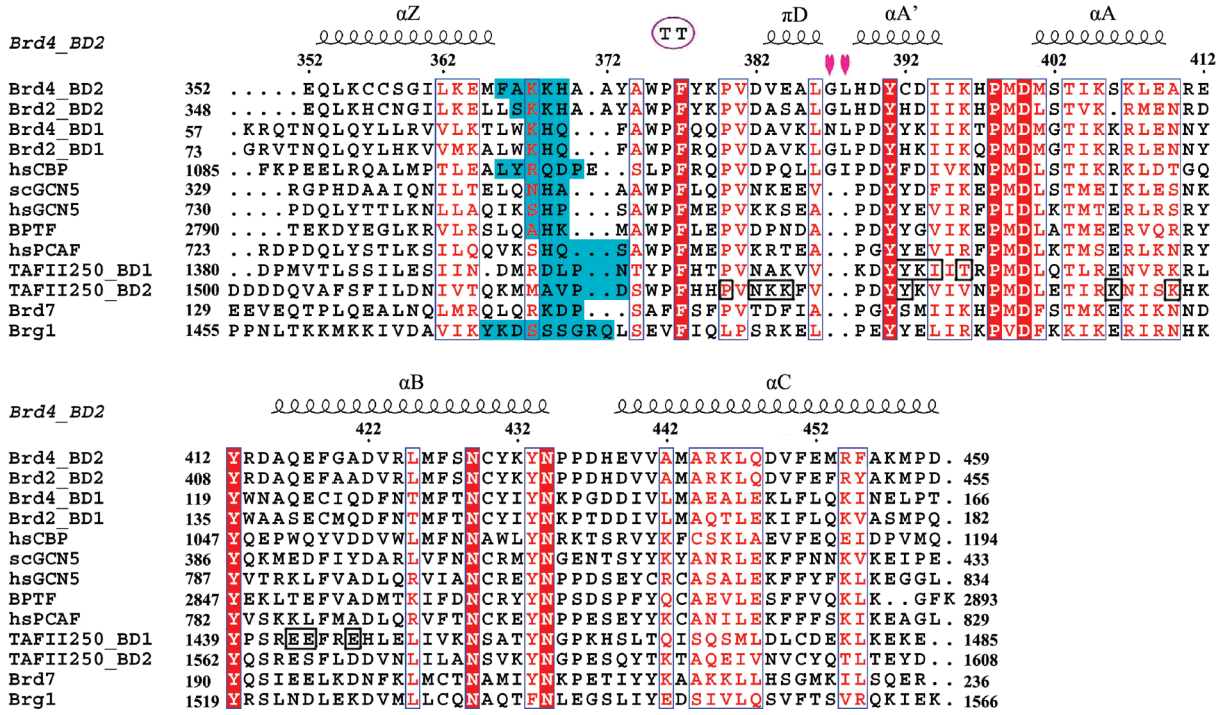

FIGURE 4: Sequence alignment of Brd4 BD2. Residues identical in all sequences are highlighted in red columns. Conserved residues are colored red in blue frames. Lowly conserved residues in αZ-αZ′ turn are in cyan columns. The residues of BDs in TAFII250, involved in heterodimerization, are indicated in black frames. Secondary structure elements for Brd4 BD2 are shown on top of the sequence, with helices as squiggles and turns as TT, surrounded by a purple ellipse for attenuation. The two amino acid insertion is indicated by pink symbols. This picture was obtained by ClustalW (*45*) and the ESPript (Easy Sequencing in PostScript) program (*46*).

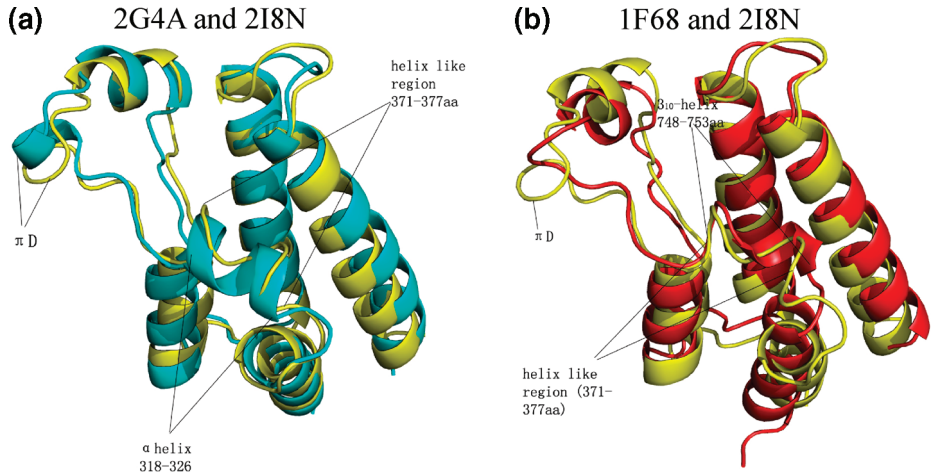

FIGURE 5: Backbone superposition of Brd4 BD2 with Brd2 BD2 and hsGCN5. (a) Average structure of Brd4 BD2 (2I8N, yellow) and Brd2 BD2 (2G4A, cyan). (b) Average structure of Brd4 BD2 (2I8N, yellow) and hsGCN5 (1F68, red).

Table 2: Peptides Used in Chemical Shift Perturbation[a]

peptide	sequence and modification
H4 (1−16)	SGRGKGGKGLGKGGAK
H4-AcK5/K12	SGRG-AcK-GGKGLG-AcK-GGAK
H3 (4−18)	KQTARKSTGGKAPRK
H3-AcK9/K14	KQTAR-AcK-STGG-AcK-APRK
H4-AcK5	SGRG-AcK-GGKG LGKGGAK
H4-AcK12	SGRGKGGKGLG-AcK-GGAK

[a] AcK denotes lysine acetylated at the ϵ-NH2.

representative ensemble. They were analyzed by the programs PROCHECK (*30*) and MOLMOL (*31*).

Chemical Shift Perturbation. NMR titrations of the BDs with peptide ligands were performed on ^{15}N-labeled proteins. ^{1}H-^{15}N HSQC spectra of free BDs were recorded as controls. Peptide ligand stock solutions of 50 mM in identical buffer were titrated stepwise with a sample dilution of less than 10%. Combined chemical shift perturbation was calculated using the following equation:

$$\Delta\delta_{ppm} = \sqrt{(\Delta\delta_{HN})^2 + (\Delta\delta_N\alpha_N)^2} \quad (1)$$

$\Delta\delta_{HN}$ and $\Delta\delta_N$ are the chemical shift variations in the proton and nitrogen dimensions, respectively. α_N, a scaling factor of 0.17, was used to normalize the ^{1}H and ^{15}N chemical shifts (*32*).

Measurement of Equilibrium Dissociation Constants. Dissociation constants, for the interaction of Brd4 BDs with different binding ligands, were obtained by monitoring the chemical shift changes of Brd4 BDs from the apo to bound form during titration. When the exchange rate is greater than the chemical shift difference between the free and bound

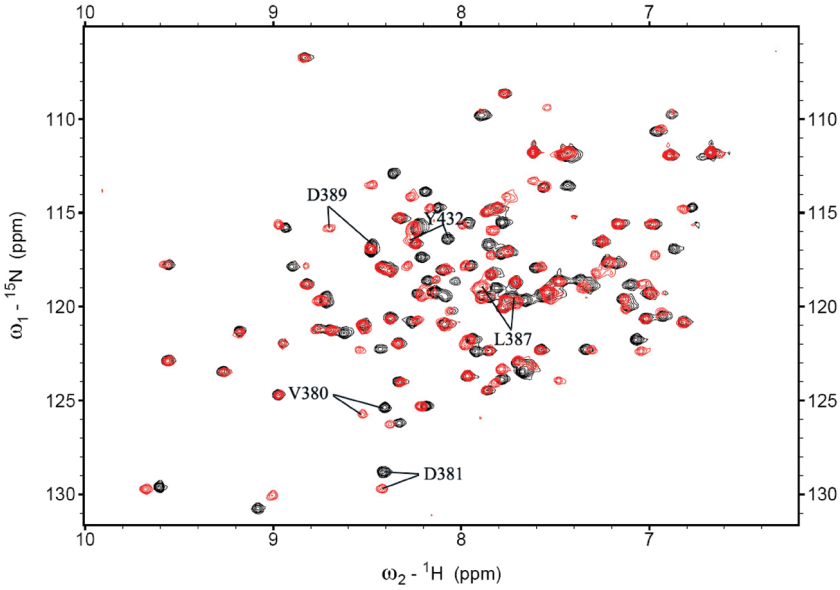

FIGURE 6: Perturbation of Brd4 BD2 by H4−K5/K12. Overlay of the ^{1}H-^{15}N HSQC spectra of Brd4 BD2 in free state (black) and in the presence of H4-AcK5/K12 peptide (red) (molar ratio of BD2/peptide = 1:8). The five residues that were selected for calculation of K_D values are denoted.

states, the observed chemical shift at each titration point, δav, is a weighted average between the chemical shifts of the free and bound states (*33–35*) obtained by the following equation:

$$\delta_{av} = \frac{[P_B]}{P_T}\delta_B + \left(1 - \frac{P_B}{P_T}\right)\delta_F \quad (2)$$

where δ_F is the chemical shift of the protein domain in the absence of a ligand, δ_B is the chemical shift of the protein domain bound to a ligand, $[P_B]$ is the concentration of Brd4 BD bound to a ligand, and $[P_T]$ is the total concentration of Brd4 BD. The mole fraction of the ligand was calculated at each titration point, and the titration curve was fitted to calculate the dissociation constant using eqs 2 and 3. In eq 3, K_D is the dissociation constant, and $[S_T]$ is the total ligand concentration at each titration point.

$$[P_B] = \frac{1}{2} \times \{(K_D + [S_T] + [P_T]) - [(K_D + [S_T] + [P_T])^2 - 4[S_T][P_T]]^{1/2}\} \quad (3)$$

Preparation and Characterization of Brd4 Bromodomain Mutants. Mutations were generated by conventional PCR method using the Brd4 BD2 construct as a template. Mutations were verified by sequencing the plasmids. BL21 (DE3) cells were transformed with the mutagenized constructs, and uniformly ^{15}N-labeled mutant proteins were produced as described in the previous section. The integrity of mutants was assessed by their ^{1}H-^{15}N HSQC spectra.

Molecular Modeling of Brd4 BD2 in Complex with H4-AcK5/K12. The structure of 2E3K is composed of four molecules of Brd2 BD2. We removed the first one that binds no peptide, and the fourth which binds to AcK5 of H4-AcK5/K12 (AcK12 is free). The remainder consists of two molecules of BD2 and one molecule of H4-AcK5/K12 with both AcK5 and AcK12 bound. It was taken as the template followed by molecular replacement. Side chain positions for H4-AcK5/K12 were determined by searching the backbone-dependent rotamer library (*36*). The complex was optimized by molecular dynamics (MD) simulations using the GROMOS96 package (*37*). The GROMOS96 force field combined with an implicit generalized-Born/solvent accessible surface area (GBSA) solvent model was used to perform the simulations. The complex was optimized by 1000 steps of steepest-descent energy minimization. Then during a 300 ps MD simulation at 300 K, all backbone heavy atoms were restrained to their respective starting positions by a harmonic potential restraint force constant of 5.0E3 KJ/(mol·nm^2). Another 500 ps MD simulation was performed on the heavy atoms of BD2 residues found outside of the peptide binding site.

NMR Backbone Relaxation Experiments and Data Analysis. ^{15}N relaxation measurements were carried out on a Bruker DMX500 NMR spectrometer by published methods (*38*). The exponential curve fitting and extracts of T1, T2, and NOE were processed by Sparky (*27*). Values of $J_e(0)$, $J(\omega_N)$, and $J(0.87\omega_H)$ were acquired by the following equations:

$$J(0.87\omega_H) = 4\sigma/(5d^2) \quad (4)$$

$$J(\omega_N) = [4R_1 - 5.00\sigma]/[3d^2 + 4c^2] \quad (5)$$

$$J_e(0) = J(0) + 6R_{ex}/[3d^2 + 4c^2] = [6R_2 - 3R_1 - 2.72\sigma]/[3d^2 + 4c^2] \quad (6)$$

where

$$\sigma = (\mathrm{NOE} - 1)R_1\gamma_N/\gamma_H \quad (7)$$

In eq 4−7, σ is the ^{1}H-^{15}N cross-relaxation rate constant; $d = [\mu_0 h\gamma_H\gamma_N/8\pi^2]r^{-3}$; $c = \omega_N\Delta\sigma/3^{1/2}$; μ_0 is the permeability of free space; h is Plank's constant; γ_H and γ_N are the gyromagnetic ratios of the ^{1}H and ^{15}N nuclei, respectively; ω_H and ω_N are the Larmor frequencies of ^{1}H and ^{15}N nuclei, respectively; r is the average internuclear ^{1}H-^{15}N distance

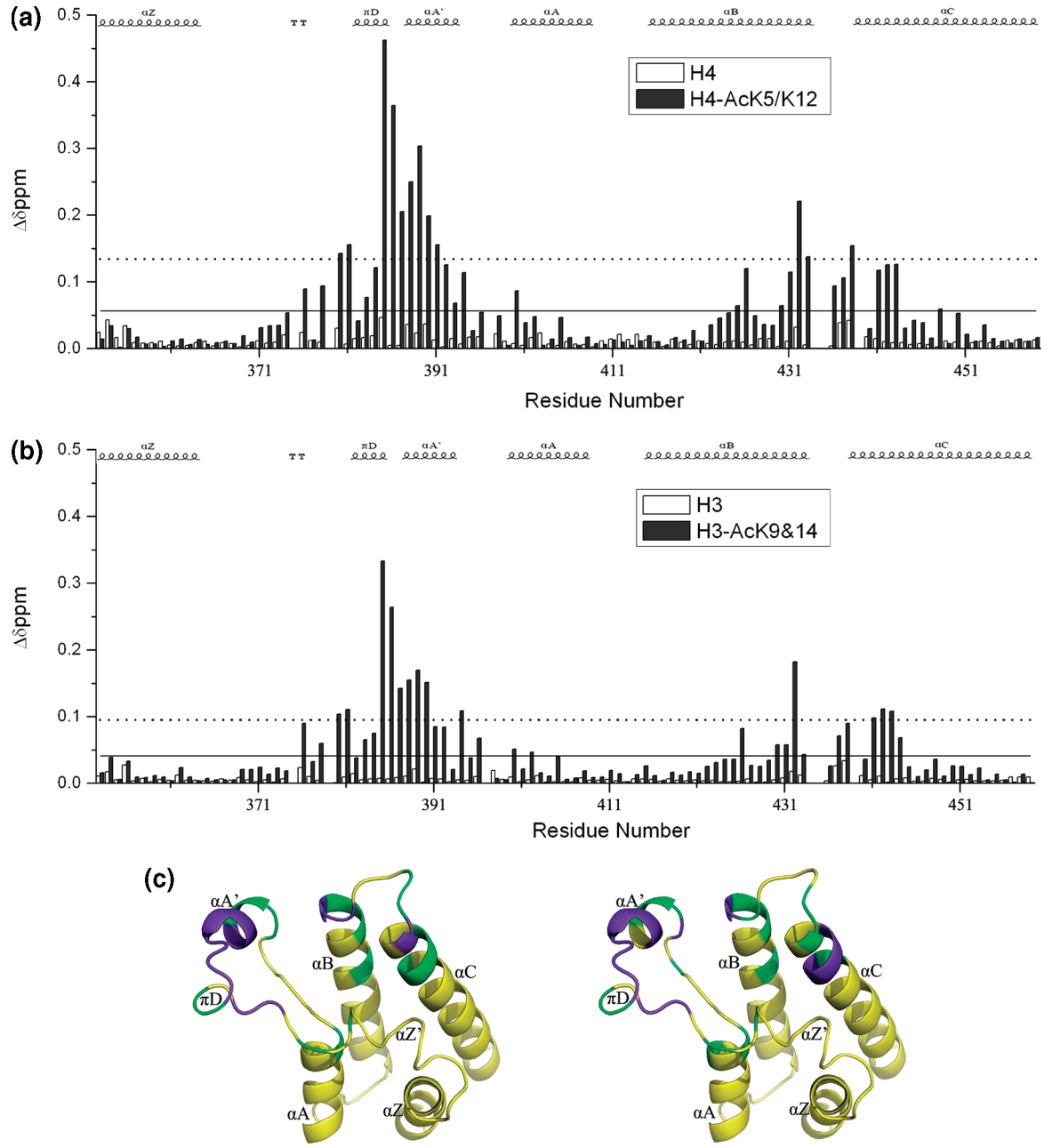

FIGURE 7: Binding properties of Brd4 BD2 with diactylated histone tails. (a) Histogram plot of combined chemical shift perturbations upon H4-AcK5/K12 saturation (black) in comparison with the H4 peptide control (white). (b) Combined chemical shift perturbations upon H3-AcK9/K14 saturation (black) in comparison with the H3 peptide control (white). The mean value is denoted as a solid line, and the mean value plus one standard deviation is denoted as a dotted line. Secondary structure elements are shown on top of the plot. (c) Ribbon diagram view mapping the binding interface of Brd4 BD2 for diacetylated H4 (left) and H3 (right) peptides. The residues perturbed significantly are colored purple, and the residues perturbed moderately are colored green.

Table 3: Perturbed Residues in Brd4 BD2[a]

	H4-AcK5/K12	H3-AcK9/K14
S	V380, D381, L385, G386, L387, H388, D389, Y390, Y432 C391,N433, E438	V380, D381, L385, G386, L387, H388, D389, Y390, Y432 I394,A441, M442, A443
M	F376, K378, E383, A384, D392, I393, M400, F426, Y430, K431, H437 I394, D436, A441, M442, A443	F376, K378, E383, A384, D392, I393, M400, F426, Y430, K431, H437 H396, T402, N433, E438, R444

[a] S means significantly perturbed resiudes, and M means moderately perturbed residues. Residues significantly perturbed by both H4 and H3 tails are colored blue. Residues moderately perturbed by both H4 and H3 tails are colored green.

(1.02 Å); and $\Delta\sigma$ is the chemical shift anisotropy (−160 ppm) (*39–42*).

Table 4: Value of K_D extracted from Chemical Shift Perturbation[a]

BD	peptide	$K_D \pm \Delta K_D$(mM)
BD1	H4-AcK5	0.81 ± 0.057
BD1	H4-AcK12	0.65 ± 0.011
BD2	H4-AcK5	1.00 ± 0.126
BD2	H4-AcK12	1.35 ± 0.078

[a] ΔK_D is the average of fitting errors from five selected residues.

RESULTS

NMR Structure Determination of Brd4 BD2. The structure of recombinant Brd4 BD2 was determined by multidimensional heteronuclear NMR spectroscopy. The 2D ^{1}H-^{15}N HSQC spectrum of BD2 showed a good dispersion of the

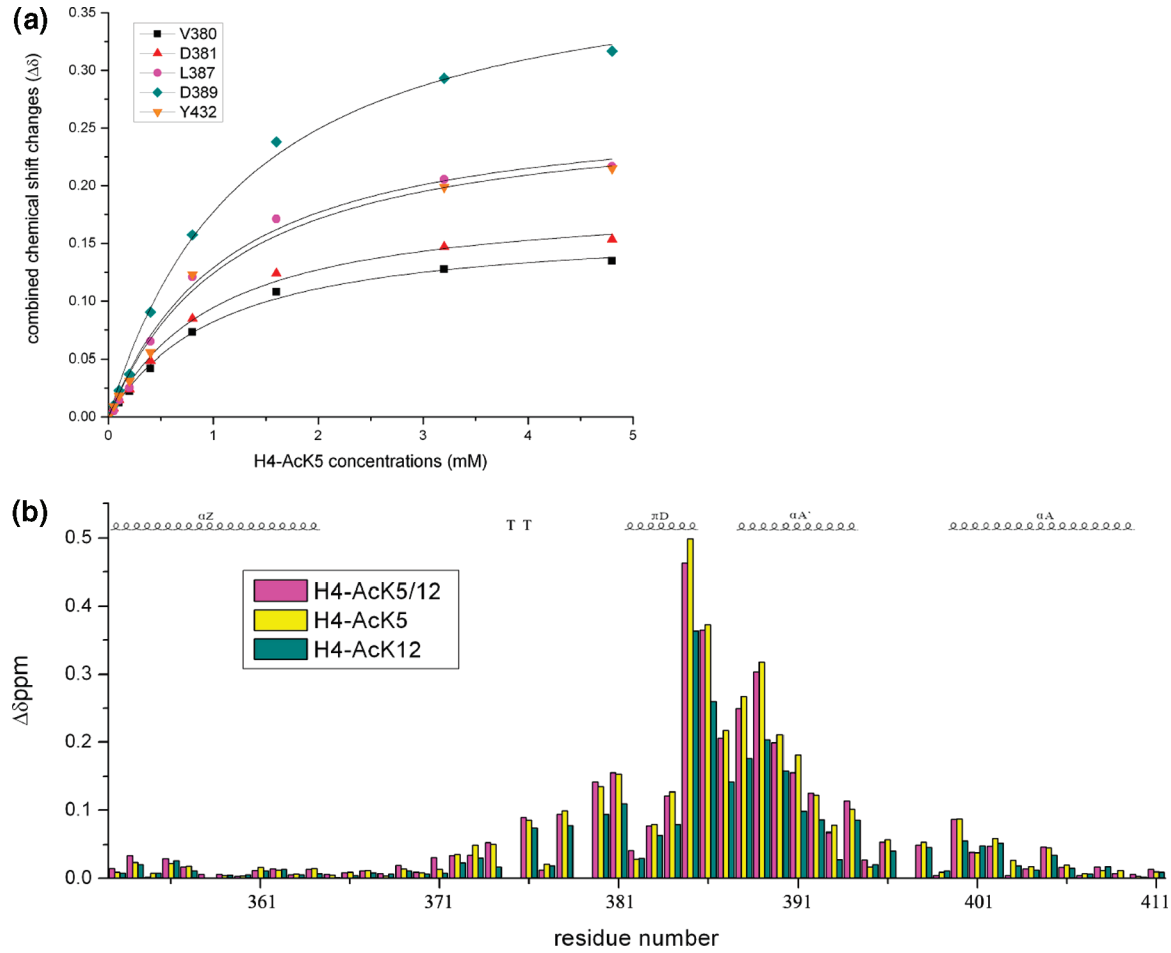

FIGURE 8: Binding properties of Brd4 BD2 with monoactylated histone tails. (a) Fitting curves of V380, D381, L387, D389, and Y432 for calculation of K_D values. Symbol and color senses are indicated in the panel. (b) Comparison of chemical shift perturbations. H4-AcK5/K12 (pink), H4-AcK5 (yellow), and H4-AcK12 (green).

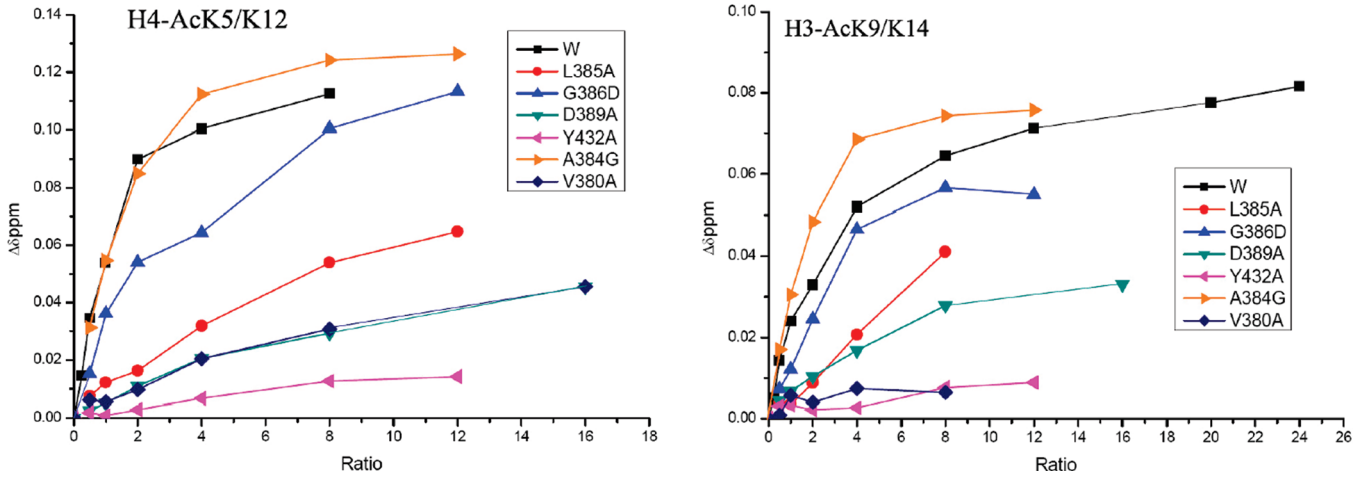

FIGURE 9: Analysis of Brd4 BD2 mutants. Chemical shift perturbations of residue F426 on wild type and mutants Brd4 BD2 upon H4-AcK5/K12 (left) and H3-AcK9/K14 (right) titration.

proton and nitrogen resonances in the amide groups (Figure 2). Ninety-nine out of the 106 total backbone residues were assigned with the exceptions of 5 proline, E352 (first residue of the recombinant), and V439. Coincidently, V435 in Brd2, the corresponding residue of V439 in Brd4, did not appear either (unpublished results). This result demonstrates the close similarity between these two proteins. A total of 1688 restraints were utilized in structure calculations, including 1490 NOE derived distance restrains, 54 hydrogen bond restraints, and 144 dihedral angle restraints. The eight residues (-LEHHHHHH) at the C-terminus as an artifact from the vector were not included in structure calculation. Table 1 lists the structural statistics for the 20 representative conformers deposited into the Protein Data Bank (ID: 2I8N). An ensemble of their backbone superimposition is shown in Figure 3a. The root-mean-square deviation (rmsd) values of the well defined secondary structure regions of the 20 structures to the average structure are 0.55 Å for the backbone and 1.29 Å for the heavy atoms. The RMSDs of total residues (E352-M457) are 0.70 Å and 1.40 Å, respec-

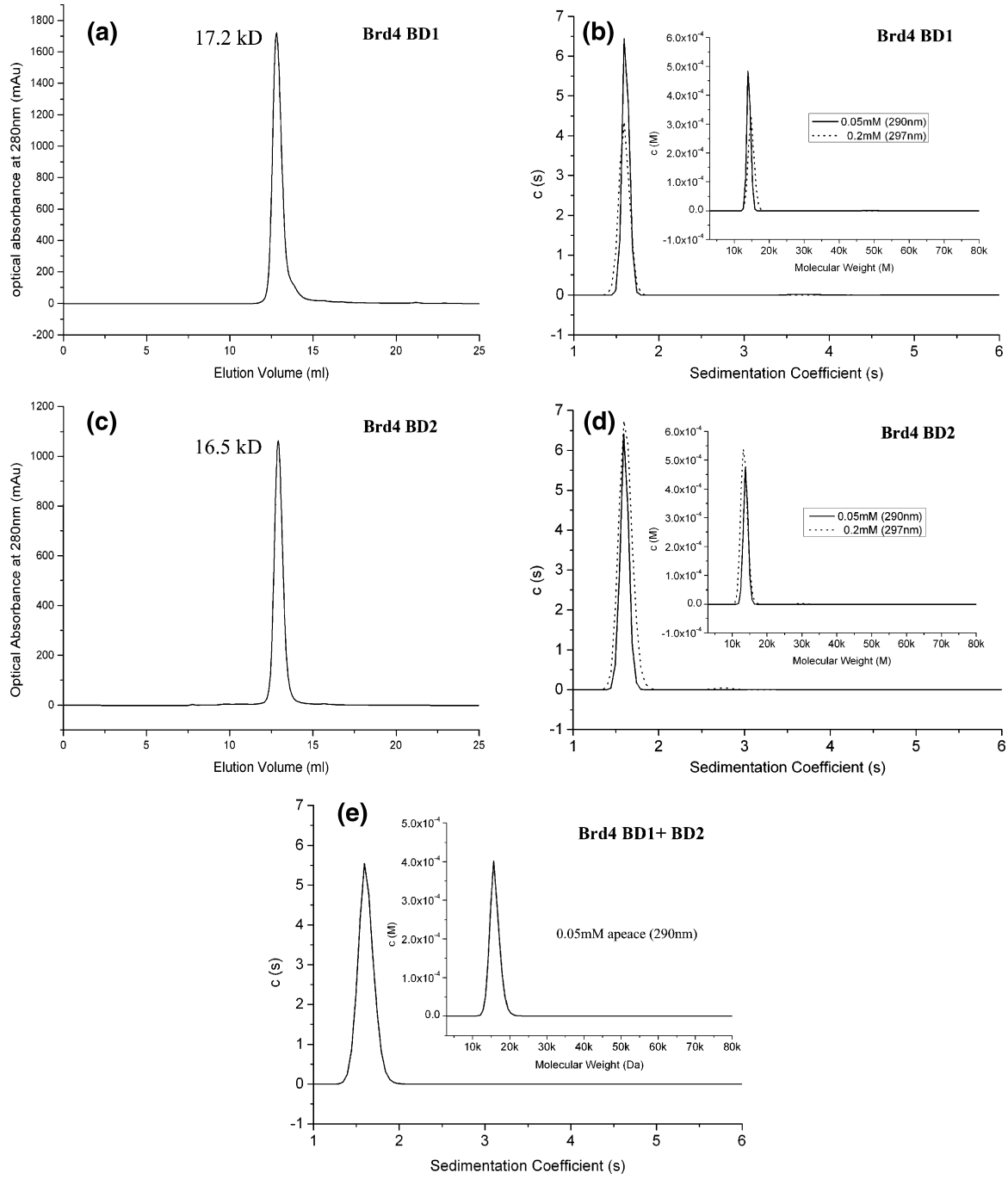

FIGURE 10: Analysis of Brd4 BDs by FPLC and AUC showed no dimerization. (a) Analysis of Brd4 BD1 by FPLC. (b) Analysis of Brd4 BD1 by AUC. (c) Analysis of Brd4 BD2 by FPLC. (d) Analysis of Brd4 BD2 by AUC. (e) Mixture of Brd4 BD1 and BD2 at equal molar values analyzed by AUC. Protein concentration and absorbance wavelength are indicated in the panels. c denotes sedimentation coefficients, s denotes Svedberg units, and M denotes molecular weight.

tively. A PROCHECK (*30*) analysis of the 20 NMR structures indicated that all of the residues lied in the most favored region and the additional allowed region of the Ramachandran plot.

Description of hBrd4 BD2 Structure. The bromodomain is a conserved ~110 amino acid module and is mainly made up of four antiparallel α-helices. Figure 3b shows the representative ribbon structure of Brd4 BD2 with the lowest energy. As expected, it contains the typical four-helix bundle of left-handed topology. They are sequentially named αZ, αA, αB, and αC from the N-terminus, corresponding to E352-M364, M400-E408, A415-Y432, and E438-M457 of the full-length protein, respectively. NOE and hydrogen bond information acquired from NMR spectroscopy demonstrated in confirmation a typical pattern for α-helical conformation in these regions. A long loop of 35 residues between αZ and αA (named ZA loop) contains two additional short helices, πD (V382-L385) and αA′ (H388-I393). Table SI-2 shows the absolute crossing angles between each two helix axis of the six. Some of the BDs also contain a 3_{10}-helix (αZ′) immediately adjacent to αZ within the long loop. In Brd2 BD2, there also exists an αZ′ (residues 364−372) that was confirmed by α helix-typical NOEs and $^{1}H-^{2}H$ exchange experiments (*43*). The corresponding region of Brd4 BD2 is limited to K368−F376 with identical sequence. Analysis of these 9 residues by TALOS (*28*) and CSI

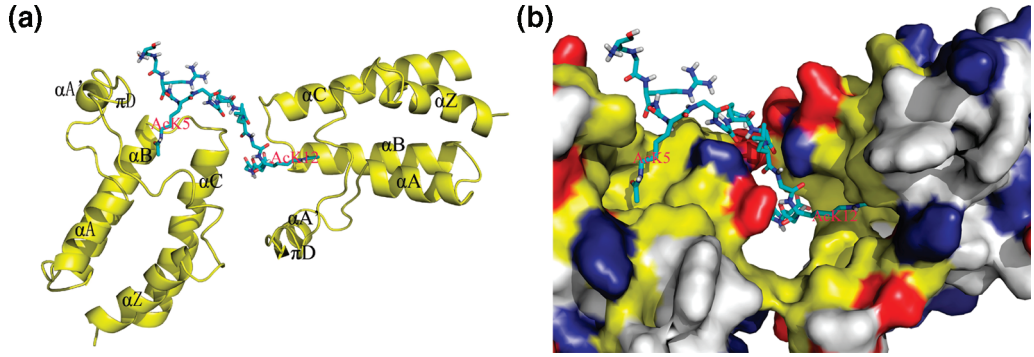

FIGURE 11: Ternary complex model of Brd4 BD2 and H4-AcK5/K12. (a) Ribbon representation of the complex model. The two acetylated lysines and the secondary structure elements of BDs are highlighted. (b) Emphasized binding surface in the same orientation as that in a. Negative residues are colored red, positive residues are colored blue, hydrophobic residues at the binding interface are colored yellow for emphasis, and other hydrophobic residues are colored white.

(Chemical shift index) (*44*) (Table SI-3) did not show α helix-typical dihedral angles or secondary structure predictions, but some helix-typical NOE constraints did exist in this region (Figure SI-4). On the $^{1}H-^{2}H$ exchange HSQC spectra, we found out that the peaks for Y372, W374, and F376 survived after 22 h, but disappeared 2 or 3 days later. Therefore, we dealt with it as an incompact αZ′ composed of a short α-helix, a two-residue turn, and a short 3_{10}-helix (see below). A shorter loop of 5 residues connects helices αB and αC (named BC loop). The ZA and BC loops pack against each other to form an electrically neutral pocket, providing a suitable surface for hydrophobic interactions (Figure 3c). This pocket is surrounded by the hydrophobic side chains of residues F376, V380, L385, L387, Y390, M398, D399, M425, F426, N428, C429, Y432, N433, and V439, providing for acetyl-lysine targeting (Figure 3d, green and white). Most of these residues are highly conserved among the BD family (Figure 4). Among them, F376, M398, M425, F426 (Figure 3d, green), and elements of the hydrophobic core line the inside bottom of this pocket. Six acidic residues (D381, D389, D392, D399, D436, and E438) (Figure 3d, red) decorate the edge of the pocket attributing to binding selectivity.

Structure Comparison with Other Bromodomains. Brd4 BD2 has much higher sequence identity with BD2 of its BET members (over 80%) than with other BDs (20−40%). Calculated by combinatorial extension (CE) (*47*), the pairwise backbone RMSDs of the solution structure of Brd4 BD2 with BD2s from BET members are between 1.4 and 1.8 Å. The RMSDs with other BDs are from 1.8 to 2.8 Å. Their overall secondary elements and structural folds are quite similar, which further proves that the left-handed, four-helix bundle is a highly conserved motif in the BD family.

The major deviations come from the loop region, especially the long ZA loop. At the entrance of this loop, there exists a turn between αZ and αZ′. The forms of this turn varied among BDs and the corresponding residues diversified through evolution (Figure 4, cyan). hsBrg1 adopts a βZ sheet (*48*), while others are irregular. Brd4 BD2 resembles Brd2 BD2 (Figure 5a) at this turn but deviates from hsGCN5 (Figure 5b) and other BDs. αZ′ is also distinctive among BDs. hsGCN5 (*49*), Brd2 BD1 (*23*), Brg1 (*48, 50*), and Brd7 (*51*) adopt a 3_{10}-helix. In Brd2 BD2, it is an α-helix (*43*). The αZ′ of Brd4 BD2 is chimeric. The first half is a short α-helix resembling the corresponding region of Brd2 BD2 (Figure 5a). The second half is a short 3_{10}-helix that resembles hsGCN5 (Figure 5b). The two parts are separated by a two-residue turn (Figure 4, purple ellipse). Besides, the unusual helix πD is formed due to the insertion of two amino acids (*43*) (Figure 4, pink symbols). It is special for BET members and CBP. Formation of the special αZ-αZ′ turn, αZ′, and πD provide Brd4 BD2 with a unique pocket for its acetylated ligands.

Binding Characteristics of Brd4 BD1 and BD2 to Histone H3 and H4 Peptides. Brd4 avidly binds to diacetylated H4-AcK5/K12 and H3-AcK9/K14 (*21*). We synthesized peptides H4 (1−16), H4-AcK5/K12, H3 (4−18), and H3-AcK9/K14 (Table 2) to titrate ^{15}N-labeled Brd4 BD2. Chemical shift changes upon H4-AcK5/K12 addition are shown in Figure 6. (Perturbation data of H3-AcK9/K14 is similar and not shown.) As expected, unmodified H4 (1−16) and H3 (4−18) barely perturbed BD2, while H4-AcK5/K12 and H3-AcK9/K14 caused significant changes. The data demonstrated a fast exchange between free and peptide-bound states of the protein in solution on NMR chemical shift time scale. Perturbed residues were distributed to ZA and BC loops, and the regions immediately flanking the BC loop. Residues with combined chemical shift changes over the mean value plus one standard deviation (Figure 7a and b, dotted line) were defined as significant ones, and those larger than the mean value (Figure 7a and b, solid line) were defined as moderate (Table 3). They were all mapped on the 3D structure in Figure 7c. Distributions of the perturbed residues were slightly different upon the binding of H4-AcK5/K12 (Figure 7c, left) and H3-AcK9/K14 (Figure 7c, right). BD2 was more perturbed by H4-AcK5/K12.

It was reported that Brd4 has comparable affinities with these two peptides and much weaker affinity with H4-AcK8/K16 (by pull-down assay) (*21*). Since BDs of Brd4 have extraordinarily high similarity with those of Brd2, their ligand selectivity should also be similar. It was also reported that Brd2 selectively interacts with H4-AcK5/K12, and with H2B to a lesser degree, and has little or no interactions with H3 and H2A (by FC-FRET) (*52*). Although different methods have distinct degrees of sensitivity, it seems unlikely for Brd4 to have a more favorable histone tail substrate than H4-AcK5/K12.

Full length Brd4 has two tandem BDs and avidly binds to diacetylated histone peptides (*21*). Since a single BD has only one pocket to accommodate one AcK, it is possible that BD1 binds to one AcK, and BD2 binds to another in

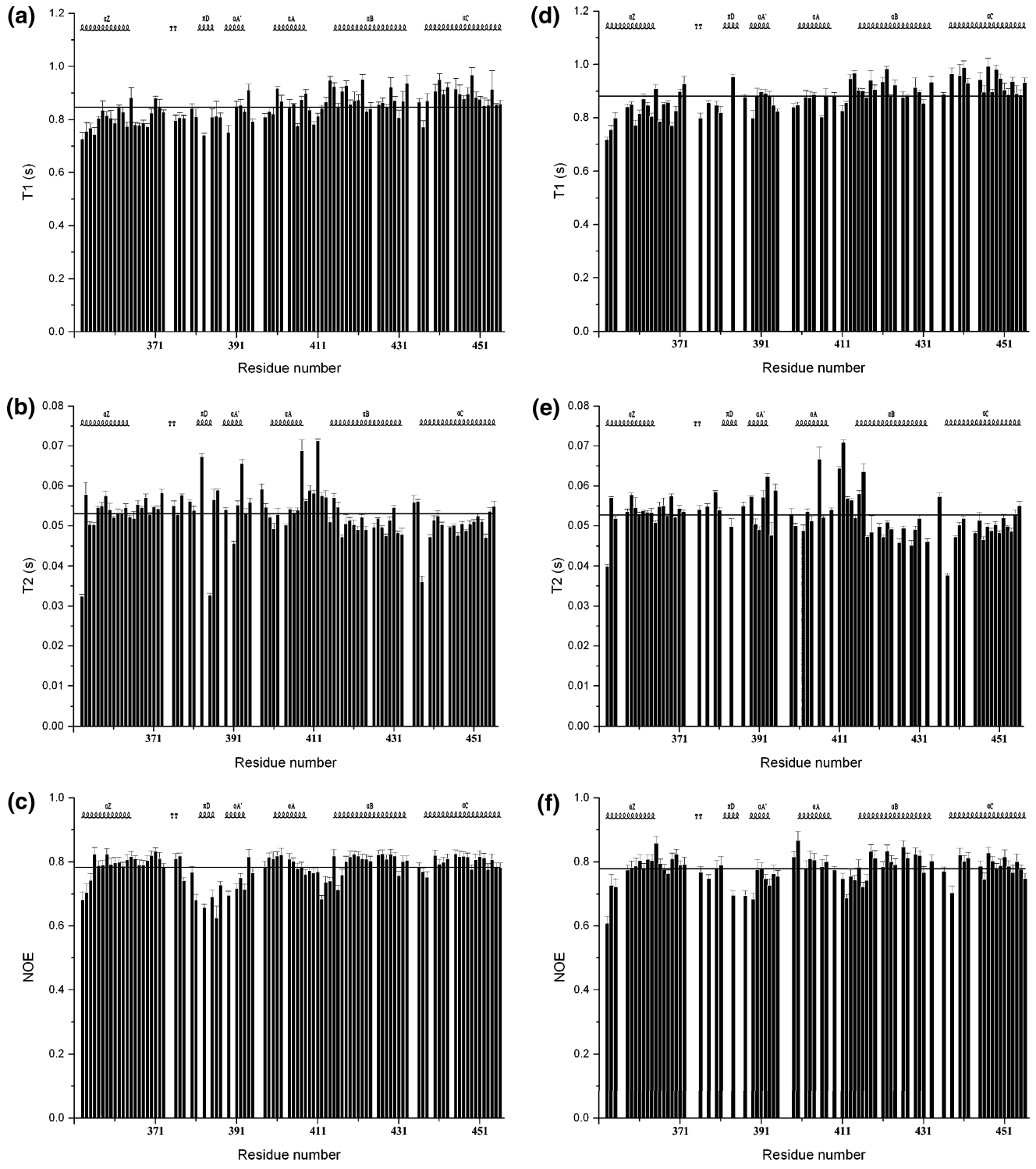

FIGURE 12: Backbone relaxation parameters of Brd4 BD2. Backbone ^{15}N T1 (a and d), T2 (b and e), and steady-state ^{1}H-^{15}N NOE (c and f) at 500 MHz are plotted against residue number. a, b, and c are for apo BD2, and d, e, and f are for H4-AcK12 saturated BD2. Standard deviations are presented as error bars.

the same histone tail. Therefore, we performed perturbation experiments with H4-AcK5 and H4-AcK12. We found that both peptides interact with BD1 and BD2. Patterns of chemical-shift perturbation for H4-AcK5 and H4-AcK12 are very similar in magnitude, direction of change, and concentration dependence. But there is a subtle difference in binding affinity (Table 4). The five most perturbed residues without severe overlap from each BD were selected to calculate the dissociation constants (K_D). Figure 8a shows the fitting curves of the five residues in BD2. Since we still have difficulty in backbone assignment of BD1, the five residues selected for BD1 are labeled as A−E in Figure SI-5. Their fitting curves were plotted in Figure SI-6. The affinity of BD1 to H4-AcK5 (0.81 mM) and H4-AcK12 (0.65 mM) is a little higher than that of BD2 (1.00 mM and 1.35 mM, respectively). Moreover, BD1 fits H4-AcK12 better than H4-AcK5. Conversely, BD2 fits H4-AcK5 better than H4-AcK12. Combined data of chemical shift changes that were acquired at H4-AcK5/K12, H4-AcK5, and H4-AcK12 saturation was plotted in Figure 8b. For most of the residues, the value of $\Delta\delta$ induced

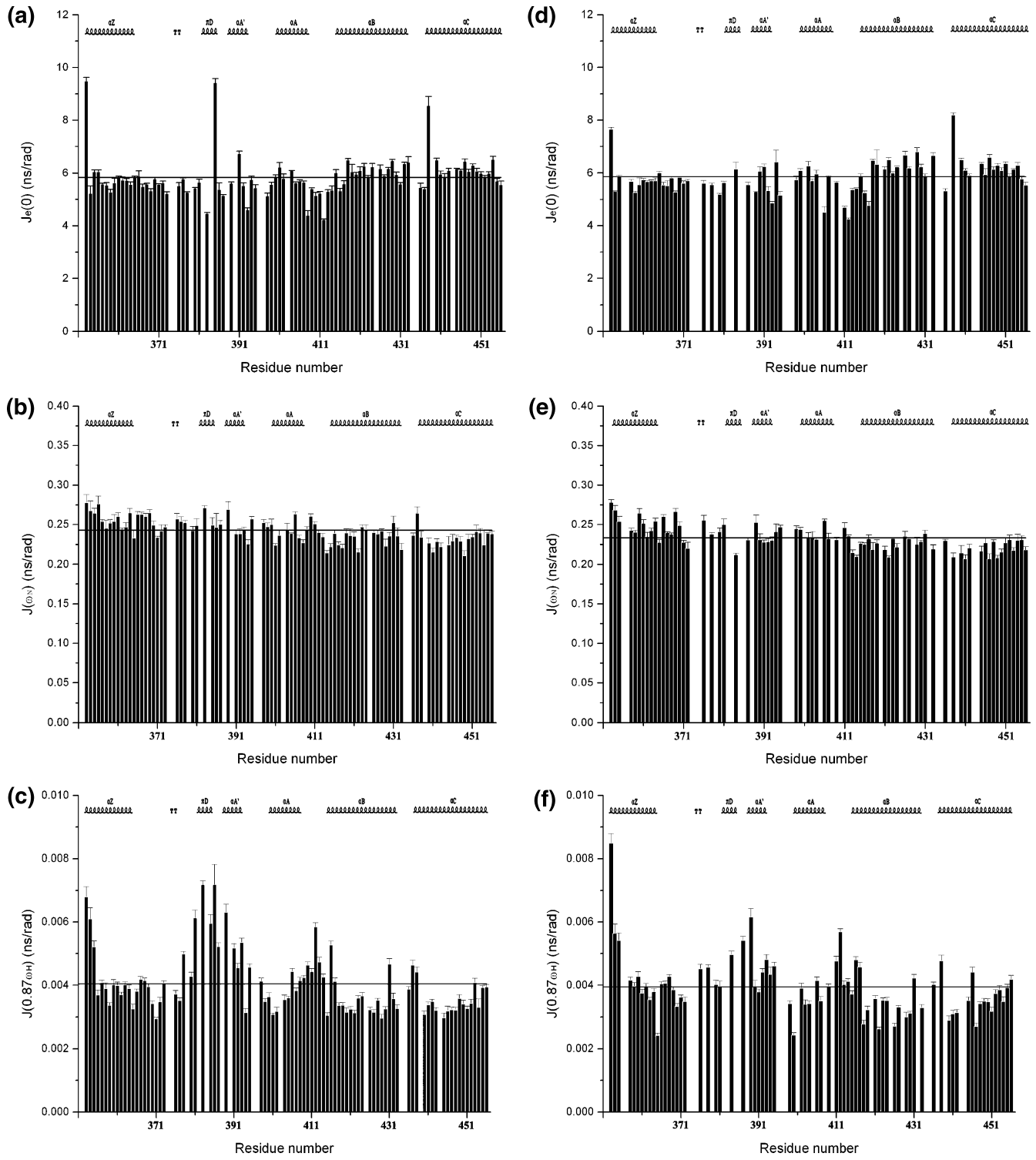

FIGURE 13: Dynamics analysis of apo and peptide bound Brd4 BD2 by reduced spectral density mapping. Values of $J_e(0)$ (a and d), $J(\omega_N)$ (b and e), and $J(0.87\omega_H)$ (c and f) are plotted against residue number. a, b, and c are for apo BD2, and d, e, and f are for H4-AcK12 saturated BD2. Standard deviations are presented as error bars.

by H4-AcK5/K12 is between that of H4-AcK5 and H4-AcK12. It suggests that, upon H4-AcK5/K12 addition, some of the BD molecules associate with AcK5 and some with AcK12. It is possible that a portion of diacetylated peptide associates with two BD molecules simultaneously, provided there is no steric hindrance. We speculate that it should be similar for diacetylated H3 peptide.

Mutational Analysis. Six mutants, L385A, G386D, D389A, Y432A, A384G, and V380A were generated to further identify how these most perturbed residues affect peptide association. Compared with wild type BD2, the ^{1}H-^{15}N HSQC spectra of mutants L385A, G386D, and A384G have moderate changes, while the other three changed a lot. HSQC spectra of L385A and Y432A are shown in Figure SI-7. Residues with ^{1}H-^{15}N resonance variations were mapped to ZA and BC loop and the flanking regions. Therefore, the chemical environment of the outer edge of the hydrophobic pocket was changed in the mutants. Since residue F426 lies

Table 5: Available K_D Values from Published Data[a]

peptide	hGCN5	peptide	TAFII250 (DBD)	peptide	PCAF
H4 K8	0.9 mM	H4 K16	39 ± 7 μM	Tat(46−55) K50	~10 μM
H4 K16	0.9 mM	H4 K8/K16	5.6 ± 0.2 μM	H4 K8	346 ± 54 μM
H2A K5	0.9 mM	H4 K5/K12	1.4 ± 0.3 μM	H4 K16	>300 μM
Ac-cntrl	0.9 mM	H4 K5/K8/K12/K16	5.3 ± 0.2 μM		

peptide	Brg1	peptide	CBP	peptide	Brd7
H3 K14	1.2 mM	p53(367−386) K382	50 μM	H3 K9	3.96 ± 0.44 mM
H4 K8	4.0 mM			H3 K14	1.19 ± 0.02 mM
H4 K12	3.6 mM			H4 K8	1.79 ± 0.10 mM
				H4 K12	3.42 ± 0.14 mM
				H4 K16	2.56 ± 0.11 mM

peptide	Brd2-2	peptide	scBdf1 (DBD)
H4 K12	2.9 mM	H4 K5/K8/K12/K16	8.4 ± 0.2 μM

[a] Peptide origin and acetylated lysine are indicated. DBD means double bromodomains.

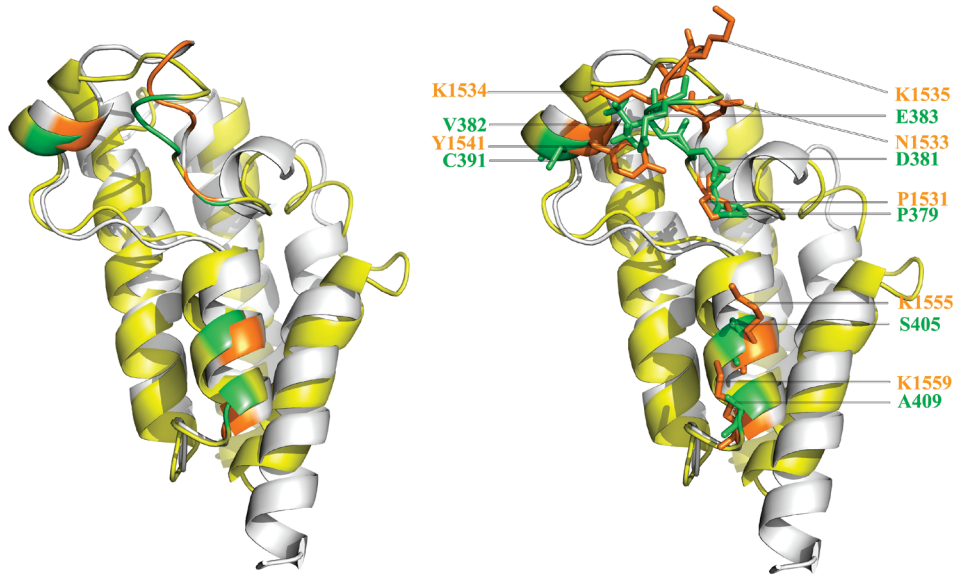

FIGURE 14: Structure comparison of TAFII250 BD2 (white) and Brd4 BD2 (yellow). Residues of TAFII250 BD2 at the heterodimeric interface are colored and labeled in orange. Corresponding residues in Brd4 BD2 are colored and labeled green.

in the bottom of the groove and is not interfered with by all of the six mutations, we utilize the value of its $\Delta\delta$ as the representative data for comparison (Figure 9). Mutant Y432A significantly impaired the recognition of both peptides, which may be attributed to severe disruption of the conformation of the binding pocket. Mutants D389A and V380A also showed greatly reduced peptide binding ability, while the binding ability of L385A and G386D was reduced to a lesser degree. In contrast, mutant A384G has higher affinity to both peptides than wild type. This residue locates in the middle of helix πD, a very important region for ligand binding. The substitution of A by G may improve the flexibility of πD and makes it more fit for acetylated peptides.

Both BDs of Brd4 Are Mainly Monomeric in Solution. We analyzed the molecular weights of BDs by FPLC size-exclusion chromatography (Figure 10a and c) and analytical ultracentrifugation (AUC) (Figure 10b and d). The collective data provided convergent evidence that, like Brd2 BD2 (*43*), purified Brd4 BD1 and BD2 are both mainly monomeric in PBS buffer (pH 7.4), which is closest to physiological conditions. No heterodimer was observed when BD1 and BD2 were mixed at equal molar values (Figure 10e).

Model of the Brd4 BD2 and H4-AcK5/K12 Complex Because Brd4 BD2 has the highest sequence similarity and closest 3D-structure with Brd2 BD2, the abridged structure of 2E3K was selected as the template for molecular dynamics (MD) simulation. The model is shown in Figure 11a, and the emphasized binding surface is shown in Figure 11b. The complex is composed of one H4-AcK5/K12 peptide and two molecules of BD2. The acetyl group of AcK5 is inserted into the hydrophobic pocket of one BD2, and the acetyl group of AcK12 is inserted into that of the other. The hydrogen bond between the carbonyl group of *N*-acetyl lysine and amide group of N433 side chain is also observed.

Dynamic Properties of Brd4 BD2. To probe the dynamic properties of Brd4 BD2 in solution, ^{15}N longitudinal (T1) and transverse (T2) relaxation times as well as steady-state ^{1}H-^{15}N NOE were measured for apo and peptide-bound states (Figure 12). Among the 99 resonance assignments, 91 of the apo state and 75 of the bound state were used in the dynamics analysis. Residues with overlapping or vanishing (L386) cross-peaks were excluded. From the average values of T1/T2, the overall rotational correlation times (τ_m) were estimated at 14.8 ns for the apo state and 15.8 ns for the peptide bound state. They are much higher than the theoreti-

cal value (~8 ns). It should not be due to protein aggregation, as suggested by analytical ultracentrifugation with the same sample (data not show). It may result from complicated anisotropic molecular tumbling (*53*) since the BD2 has a special long ZA loop. Therefore, the relaxation data cannot be interpreted by the usual model-free approach. The reduced spectral density mapping formalism was applied instead since it makes no assumptions about the nature of the rotational diffusion. Values of spectral density function at $\omega = 0$, ω_N and $0.87\omega_H$, were derived and plotted in Figure 13 (*41, 42*). For apo-state BD2, Q353 (at the beginning of αZ), L385 (at the end of πD), and E438 (at the end of BC loop) exhibited much lower T2 values (Figure 12b) and significantly higher $J_e(0)$ (Figure 13a) than the average, suggesting distinct microsecond−millisecond exchange processes. Since L385 overlapped with the R410 at H4-AcK12 saturated state, its relaxation data is not available. But for peptide-bound BD2, available Q353 and E438 exhibited higher T2 (Figure 12b and e) and lower $J_e(0)$ (Figure 13a and d), compared with the apo state. This suggested that ligand binding depressed the conformational exchanges to some degree. The depression was not limited to the binding site, but was also in the distant regions. L385 should also be similarly affected. The values of $J(\omega_N)$ show less variation with residue number, with typical values between 0.25 and 0.35 ns. The $J(0.87\omega_H)$ values of residue 353−355, 378−393, 395, 398, 406, 408−414, 416, 417, 431, 437, and 438 are higher than the average, indicating fast internal motions on the picosecond−nanosecond time scale. These residues locate either at the loop regions or at the beginning of α-helices flanking the loops. Their relatively lower NOEs also reconfirm their high flexibility. The fast internal motions were affected irregularly upon peptide binding. At the binding site, $J(0.87\omega_H)$ of D381 decreased a lot, and $J(0.87\omega_H)$ of E438 increased a little upon peptide binding (Figure 13c and f). The same complications were also observed in other regions.

DISCUSSION

The solution structure of Brd4 BD2 shows the conserved left-handed, four-helix bundle scaffold. But the special αZ-αZ′ turn, the incompact αZ′, helix πD, together with other decorations on ZA and BC loops present a unique surface on the functional pocket, which determines the selectivity and binding affinity of the substrate.

We demonstrated that H4-AcK5 and H4-AcK12 bind to both BDs of Brd4. Their K_D values were estimated (Table 4). Along with the published K_D values listed in Table 5, we noticed that most BDs have a broad specificity for histone peptides. However, a particular lysine-acetylated histone tail can be recognized by several BDs. Generally, the bindings are rather weak, with K_D values in the milimolar scale for individual BDs. For monomeric BDs, only CBP and PCAF have K_D values in the micromolar scale. But it is worth noting that their ligands of high affinity are not from histone tails. The histone peptide substrates of PCAF still have K_D values in the milimolar scale. In contrast, the double BD pairs (TAFII250, scBdf1, and probably Brd2 BD1) all have much higher affinity for histone tails. Their K_D values were estimated on the micromolar scale.

The negatively charged cavity engendered upon dimerization of Brd2 BD1 was speculated to be a potential secondary binding site for a basic residue of the acetylated histone H4 tail, which endows the dimer with a higher affinity for the substrate than the mutated monomer (*23*). On the basis of the dimeric structure of Brd2 BD1, it was predicted that a secondary binding pocket may also form by homo- or hetero-dimerization of Brd4 BDs and help to determine the binding specificity and affinity (*9*). The amino acids in human Brd4 potentially involved in homodimeric interactions were also pointed out (*9*). But our results suggested that BDs of Brd4 do not form homo- or hetero-dimers. Hence, no secondary binding pocket exists in Brd4.

For the double BD module of human TAFII250, there is an interaction interface between the two BDs (*54*). Residues contributing to the heterodimeric interface are indicated in Figure 4 (black frame). The corresponding residues in Brd4 differ significantly. Structure comparison of corresponding residues of BD2 from TAFII250 and Brd4 are shown in Figure 14. Obvious variations can be seen not only on side chain properties but also on the configuration in the 3D structures. Therefore, BDs of Brd4 do not form a heterodimer as TAFII250. Moreover, there are only 14 residues between the two BDs of TAFII250, which may bring the two domains into close contact. But the linker of BDs in Brd4 contains 183 residues and lacks secondary structures, as predicted by GOR4 (*55*). The fragment of Brd4 (residues 49−457) containing the two BDs and the long linker severely degrades in solution. Many bands from degradation were observed by SDS−PAGE immediately after the protein was purified. After further incubation at room temperature for about 2 days, it was completely degraded into smaller fragments. In contrast, the two fragments of separately isolated BDs both hold a durative stability against degradation. These results suggest that without other cofactors, the linker should be exposed to the solution environment and be ready for incision by proteinase. It might look like an extended strand (the linker) with two balls (the independent BDs) at both ends.

Individual BD of Brd4 bears weak interactions with acetylated histone tails, and Brd4 fails to form a homo- or hetero-dimer through its BDs. This protein should have its own mechanism to hold onto chromosomes during mitosis and regulation of associated cellular processes. Other proteins or protein complexes may contribute to the attachment. Papillomavirus E2 sets up a good model for reinforcement of Brd4 and acetyl-chromatin association. Brd4 and E2 enhance each other's association with chromatin mutually (*20*). It was suggested that acetylation alone is not sufficient to stabilize Brd4 binding to chromatin and that a sequence specific DNA-binding protein like E2 is also needed (*9*). Besides, Brd4 was found to present in selective forms of mediator complexes (*1, 6–9*). Components of the mediator complex may also strengthen the association of Brd4 to the acetylated chromatin.

ACKNOWLEDGMENT

We thank Dr. Yinshan Yang (INSERM, U554, Centre de Biochimie Structurale, 29, rue de Navacelles, F-34090 Montpellier, France) for excellent technical assistance in NMR experiments; Professor Luhua Lai (PKU, China) and Dr. Ping Wei (PKU, China) for the assistance with the analytical ultracentrifugation experiments; and Dr. Jin Han (University of Chicago, HHMI, Chicago, IL 60637, America),

Dr. Weiqun Shen, Qi Hu, Fangming Wu, and Xingsheng Wang for constructive advice regarding manuscript preparation. We also thank all the other members in our laboratory, past and present, who have contributed to this work. We thank Dr. F. Delaglio and Professor A. Bax for providing the software NMRPipe, Professors T. D. Goddard and D. G. Kneller for providing Sparky, Professor A. T. Brünger for providing the program CNS, Dr. R. Koradi and Professor K. Wüthrich for providing MOLMOL, M. Carson for providing Ribbons, and Dr. W. L. DeLano for providing PyMOL.

SUPPORTING INFORMATION AVAILABLE

Primers used in the polymerase chain reaction; the absolute crossing angles between each helix of Brd4 BD2; analysis of Brd4 BD2 (368−376) by TALOS and Csi; summary of sequential and medium-range NOE connectivities observed in Brd4 BD2; overlay of the ^{1}H-^{15}N HSQC spectra of Brd4 BD1 in apo and bound state; fitting curves of A-E of Brd4 BD1 for extraction of K_D; and overlay of HSQC spectra of mutant L385A and Y432A with wild type BD2. This material is available free of charge via the Internet at http://pubs.acs.org.

REFERENCES

1. Jang, M. K., Mochizuki, K., Zhou, M., Jeong, H. S., Brady, J. N., and Ozato, K. (2005) The bromodomain protein Brd4 is a positive regulatory component of P-TEFb and stimulates RNA polymerase II-dependent transcription. *Mol. Cell 19*, 523–534.
2. Yang, Z., Yik, J. H., Chen, R., He, N., Jang, M. K., Ozato, K., and Zhou, Q. (2005) Recruitment of P-TEFb for stimulation of transcriptional elongation by the bromodomain protein Brd4. *Mol. Cell 19*, 535–545.
3. Bisgrove, D. A., Mahmoudi, T., Henklein, P., and Verdin, E. (2007) Conserved P-TEFb-interacting domain of BRD4 inhibits HIV transcription. *Proc. Natl. Acad. Sci. U.S.A. 104*, 13690–13695.
4. Maruyama, T., Farina, A., Dey, A., Cheong, J., Bermudez, V. P., Tamura, T., Sciortino, S., Shuman, J., Hurwitz, J., and Ozato, K. (2002) A Mammalian bromodomain protein, brd4, interacts with replication factor C and inhibits progression to S phase. *Mol. Cell. Biol. 22*, 6509–6520.
5. Farina, A., Hattori, M., Qin, J., Nakatani, Y., Minato, N., and Ozato, K. (2004) Bromodomain protein Brd4 binds to GTPase-activating SPA-1, modulating its activity and subcellular localization. *Mol. Cell. Biol. 24*, 9059–9069.
6. Jiang, Y. W., Veschambre, P., Erdjument-Bromage, H., Tempst, P., Conaway, J. W., Conaway, R. C., and Kornberg, R. D. (1998) Mammalian mediator of transcriptional regulation and its possible role as an end-point of signal transduction pathways. *Proc. Natl. Acad. Sci. U.S.A. 95*, 8538–8543.
7. Houzelstein, D., Bullock, S. L., Lynch, D. E., Grigorieva, E. F., Wilson, V. A., and Beddington, R. S. (2002) Growth and early postimplantation defects in mice deficient for the bromodomain-containing protein Brd4. *Mol. Cell. Biol. 22*, 3794–3802.
8. Wu, S. Y., Zhou, T., and Chiang, C. M. (2003) Human mediator enhances activator-facilitated recruitment of RNA polymerase II and promoter recognition by TATA-binding protein (TBP) independently of TBP-associated factors. *Mol. Cell. Biol. 23*, 6229–6242.
9. Wu, S. Y., and Chiang, C. M. (2007) The double bromodomain-containing chromatin adaptor Brd4 and transcriptional regulation. *J. Biol. Chem. 282*, 13141–13145.
10. Ottinger, M., Christalla, T., Nathan, K., Brinkmann, M. M., Viejo-Borbolla, A., and Schulz, T. F. (2006) Kaposi's sarcoma-associated herpesvirus LANA-1 interacts with the short variant of BRD4 and releases cells from a BRD4- and BRD2/RING3-induced G1 cell cycle arrest. *J. Virol. 80*, 10772–10786.
11. You, J., Srinivasan, V., Denis, G. V., Harrington, W. J.Jr., Ballestas, M. E., Kaye, K. M., and Howley, P. M. (2006) Kaposi's sarcoma-associated herpesvirus latency-associated nuclear antigen interacts with bromodomain protein Brd4 on host mitotic chromosomes. *J. Virol. 80*, 8909–8919.
12. You, J., Croyle, J. L., Nishimura, A., Ozato, K., and Howley, P. M. (2004) Interaction of the bovine papillomavirus E2 protein with Brd4 tethers the viral DNA to host mitotic chromosomes. *Cell 117*, 349–360.
13. Ilves, I., Maemets, K., Silla, T., Janikson, K., and Ustav, M. (2006) Brd4 is involved in multiple processes of the bovine papillomavirus type 1 life cycle. *J. Virol. 80*, 3660–3665.
14. McPhillips, M. G., Oliveira, J. G., Spindler, J. E., Mitra, R., and McBride, A. A. (2006) Brd4 is required for e2-mediated transcriptional activation but not genome partitioning of all papillomaviruses. *J. Virol. 80*, 9530–9543.
15. Schweiger, M. R., You, J., and Howley, P. M. (2006) Bromodomain protein 4 mediates the papillomavirus E2 transcriptional activation function. *J. Virol. 80*, 4276–4285.
16. Cho, W. K., Zhou, M., Jang, M. K., Huang, K., Jeong, S. J., Ozato, K., and Brady, J. N. (2007) Modulation of the Brd4/P-TEFb interaction by the human T-lymphotropic virus type 1 tax protein. *J. Virol. 81*, 11179–11186.
17. Paillisson, A., Levasseur, A., Gouret, P., Callebaut, I., Bontoux, M., Pontarotti, P., and Monget, P. (2007) Bromodomain testis-specific protein is expressed in mouse oocyte and evolves faster than its ubiquitously expressed paralogs BRD2,−3, and−4. *Genomics 89*, 215–223.
18. Abbate, E. A., Voitenleitner, C., and Botchan, M. R. (2006) Structure of the papillomavirus DNA-tethering complex E2:Brd4 and a peptide that ablates HPV chromosomal association. *Mol. Cell 24*, 877–889.
19. Rechsteiner, M., and Rogers, S. W. (1996) PEST sequences and regulation by proteolysis. *Trends Biochem. Sci. 21*, 267–271.
20. Wu, S. Y., Lee, A. Y., Hou, S. Y., Kemper, J. K., Erdjument-Bromage, H., Tempst, P., and Chiang, C. M. (2006) Brd4 links chromatin targeting to HPV transcriptional silencing. *Genes Dev. 20*, 2383–2396.
21. Dey, A., Chitsaz, F., Abbasi, A., Misteli, T., and Ozato, K. (2003) The double bromodomain protein Brd4 binds to acetylated chromatin during interphase and mitosis. *Proc. Natl. Acad. Sci. U.S.A. 100*, 8758–8763.
22. Dey, A., Ellenberg, J., Farina, A., Coleman, A. E., Maruyama, T., Sciortino, S., Lippincott-Schwartz, J., and Ozato, K. (2000) A bromodomain protein, MCAP, associates with mitotic chromosomes and affects G(2)-to-M transition. *Mol. Cell. Biol. 20*, 6537–6549.
23. Nakamura, Y., Umehara, T., Nakano, K., Jang, M. K., Shirouzu, M., Morita, S., Uda-Tochio, H., Hamana, H., Terada, T., Adachi, N., Matsumoto, T., Tanaka, A., Horikoshi, M., Ozato, K., Padmanabhan, B., and Yokoyama, S. (2007) Crystal structure of the human BRD2 bromodomain: insights into dimerization and recognition of acetylated histone H4. *J. Biol. Chem. 282*, 4193–4201.
24. Schuck, P. (2000) Size-distribution analysis of macromolecules by sedimentation velocity ultracentrifugation and lamm equation modeling. *Biophys. J. 78*, 1606–1619.
25. Schuck, P. (2003) On the analysis of protein self-association by sedimentation velocity analytical ultracentrifugation. *Anal. Biochem. 320*, 104–124.
26. Delaglio, F., Grzesiek, S., Vuister, G. W., Zhu, G., Pfeifer, J., and Bax, A. (1995) NMRPipe: a multidimensional spectral processing system based on UNIX pipes. *J. Biomol. NMR 6*, 277–293.
27. Goddard, T. D., and Kneller, D. G. (2006) *Sparky 3*, University of California, San Francisco, CA.
28. Cornilescu, G., Delaglio, F., and Bax, A. (1999) Protein backbone angle restraints from searching a database for chemical shift and sequence homology. *J. Biomol. NMR 13*, 289–302.
29. Brunger, A. T., Adams, P. D., Clore, G. M., DeLano, W. L., Gros, P., Grosse-Kunstleve, R. W., Jiang, J. S., Kuszewski, J., Nilges, M., Pannu, N. S., Read, R. J., Rice, L. M., Simonson, T., and Warren, G. L. (1998) Crystallography & NMR system: A new software suite for macromolecular structure determination. *Acta Crystallogr., Sect. D 54*, 905–921.
30. Laskowski, R. A., Rullmannn, J. A., MacArthur, M. W., Kaptein, R., and Thornton, J. M. (1996) AQUA and PROCHECK-NMR: programs for checking the quality of protein structures solved by NMR. *J. Biomol. NMR 8*, 477–486.
31. Koradi, R., Billeter, M., and Wuthrich, K. (1996) MOLMOL: a program for display and analysis of macromolecular structures. *J. Mol. Graphics 14*, 51–55; 29−32.
32. Tochio, H., Zhang, Q., Mandal, P., Li, M., and Zhang, M. (1999) Solution structure of the extended neuronal nitric oxide synthase

PDZ domain complexed with an associated peptide. *Nat. Struct. Biol. 6*, 417–421.
33. Lian, L. Y., Barsukov, I. L., Sutcliffe, M. J., Sze, K. H., and Roberts, G. C. (1994) Protein-ligand interactions: exchange processes and determination of ligand conformation and protein-ligand contacts. *Methods Enzymol. 239*, 657–700.
34. Liu, D., Prasad, R., Wilson, S. H., DeRose, E. F., and Mullen, G. P. (1996) Three-dimensional solution structure of the N-terminal domain of DNA polymerase beta and mapping of the ssDNA interaction interface. *Biochemistry 35*, 6188–6200.
35. Hu, H. Y., Horton, J. K., Gryk, M. R., Prasad, R., Naron, J. M., Sun, D. A., Hecht, S. M., Wilson, S. H., and Mullen, G. P. (2004) Identification of small molecule synthetic inhibitors of DNA polymerase beta by NMR chemical shift mapping. *J. Biol. Chem. 279*, 39736–39744.
36. Dunbrack, R. L., Jr., and Karplus, M. (1993) Backbone-dependent rotamer library for proteins. Application to side-chain prediction. *J. Mol. Biol. 230*, 543–574.
37. Van Gunstern, W. F., Billeter, S. R., Eising, A. A., Hunenberger, P. H., Kruger, P., Mark, A. E., Scott, W. R., and Tironi, I. G. (1996) *Biomolecular Simulation: The GROMOS96 Manual and User Guide*, Vdf Hochschulverlag, Zurich, Switzerland.
38. Farrow, N. A., Muhandiram, R., Singer, A. U., Pascal, S. M., Kay, C. M., Gish, G., Shoelson, S. E., Pawson, T., Forman-Kay, J. D., and Kay, L. E. (1994) Backbone dynamics of a free and phosphopeptide-complexed Src homology 2 domain studied by 15N NMR relaxation. *Biochemistry 33*, 5984–6003.
39. Yukio Hiyama, C. H. N., James V., Silverton., Alfonso, Bavoso., and Dennis A., Torchia. (1988) Determination of 15N chemical shift tensor via 15N-2H dipolar coupling in Bocglycyl-glycyl [15N]glycine benzyl ester. *J. Am. Chem. Soc. 110*, 2378–2383.
40. Farrow, N. A., Zhang, O., Forman-Kay, J. D., and Kay, L. E. (1995) Comparison of the backbone dynamics of a folded and an unfolded SH3 domain existing in equilibrium in aqueous buffer. *Biochemistry 34*, 868–878.
41. Farrow, N. A., Zhang, O., Szabo, A., Torchia, D. A., and Kay, L. E. (1995) Spectral density function mapping using 15N relaxation data exclusively. *J. Biomol. NMR 6*, 153–162.
42. Fairbrother, W. J., Liu, J., Pisacane, P. I., Sliwkowski, M. X., and Palmer, A. G., 3rd (1998) Backbone dynamics of the EGF-like domain of heregulin-alpha. *J. Mol. Biol. 279*, 1149–1161.
43. Huang, H., Zhang, J., Shen, W., Wang, X., Wu, J., and Shi, Y. (2007) Solution structure of the second bromodomain of Brd2 and its specific interaction with acetylated histone tails. *BMC Struct. Biol. 7*, 57.
44. Wishart, D. S., and Sykes, B. D. (1994) The 13C chemical-shift index: a simple method for the identification of protein secondary structure using 13C chemical-shift data. *J. Biomol. NMR 4*, 171–180.
45. Thompson, J. D., Higgins, D. G., and Gibson, T. J. (1994) CLUSTAL W: improving the sensitivity of progressive multiple sequence alignment through sequence weighting, position-specific gap penalties and weight matrix choice. *Nucleic Acids Res. 22*, 4673–4680.
46. Gouet, P., Courcelle, E., Stuart, D. I., and Metoz, F. (1999) ESPript: analysis of multiple sequence alignments in PostScript. *Bioinformatics 15*, 305–308.
47. Shindyalov, I. N., and Bourne, P. E. (1998) Protein structure alignment by incremental combinatorial extension (CE) of the optimal path. *Protein Eng. 11*, 739–747.
48. Singh, M., Popowicz, G. M., Krajewski, M., and Holak, T. A. (2007) Structural ramification for acetyl-lysine recognition by the bromodomain of human BRG1 protein, a central ATPase of the SWI/SNF remodeling complex. *ChemBioChem 8*, 1308–1316.
49. Hudson, B. P., Martinez-Yamout, M. A., Dyson, H. J., and Wright, P. E. (2000) Solution structure and acetyl-lysine binding activity of the GCN5 bromodomain. *J. Mol. Biol. 304*, 355–370.
50. Shen, W., Xu, C., Huang, W., Zhang, J., Carlson, J. E., Tu, X., Wu, J., and Shi, Y. (2007) Solution structure of human Brg1 bromodomain and its specific binding to acetylated histone tails. *Biochemistry 46*, 2100–2110.
51. Sun, H., Liu, J., Zhang, J., Shen, W., Huang, H., Xu, C., Dai, H., Wu, J., and Shi, Y. (2007) Solution structure of BRD7 bromodomain and its interaction with acetylated peptides from histone H3 and H4. *Biochem. Biophys. Res. Commun. 358*, 435–441.
52. Kanno, T., Kanno, Y., Siegel, R. M., Jang, M. K., Lenardo, M. J., and Ozato, K. (2004) Selective recognition of acetylated histones by bromodomain proteins visualized in living cells. *Mol. Cell 13*, 33–43.
53. Viles, J. H., Donne, D., Kroon, G., Prusiner, S. B., Cohen, F. E., Dyson, H. J., and Wright, P. E. (2001) Local structural plasticity of the prion protein. Analysis of NMR relaxation dynamics. *Biochemistry 40*, 2743–2753.
54. Jacobson, R. H., Ladurner, A. G., King, D. S., and Tjian, R. (2000) Structure and function of a human TAFII250 double bromodomain module. *Science 288*, 1422–1425.
55. Combet, C., Blanchet, C., Geourjon, C., and Deleage, G. (2000) NPS@: network protein sequence analysis. *Trends Biochem. Sci. 25*, 147–150.

BI8001659